Theoretical Drag Prediction for Trailing Decelerators at Supersonic Speeds

THOMAS W. BRUNNER*
Goodyear Aerospace Corporation, Akron, Ohio

AND

ROBERT M. NEREM†
Ohio State University, Columbus, Ohio

The development of a method for predicting decelerator performance has been under investigation for several years. The present state of this program allows for the prediction of drag for a trailing decelerator in a supersonic flow and at zero angle of attack. These drag calculations are made using recently developed methods for computing flowfields into and around trailing decelerators in conjunction with empirical correlations to define base-pressure drag. The details of the flowfield computations are briefly summarized, and initial results leading to drag prediction for balloon-parachutes (Ballutes)‡ and parachutes are examined and compared with experimental data.

Nomenclature

C_D = drag coefficient
C_{D_0} = total drag coefficient
C_P = pressure coefficient
D = forebody diameter
d = decelerator projected diameter
d_0 = parachute nominal diameter
d_R = reefed diameter
d_w = wake diameter
M = Mach number
P = pressure
R_S = distance to dividing streamline
r = radial distance
S = surface area
V = velocity
X = axial distance
γ = ratio of specific heats
λ = effective material porosity
λ_g = geometric porosity
ρ = density
ψ = streamline
ψ_D = dividing streamline

Subscripts

B = body base
BF = burble fence
E = exterior surface
F = Ballute forebody
I = interior surface
max = maximum
P = parachute
s = plateau pressure, shock
T = Ballute
t = total conditions
w = wake conditions
1 = conditions at flow separation
2 = conditions just downstream of a normal shock
∞ = freestream conditions
* = critical conditions

Presented as Paper 70-1177 at the AIAA Aerodynamic Deceleration Systems Conference, Dayton, Ohio, September 14–16, 1970; submitted October 5, 1970; revision received April 28, 1971.

Index category: Post-Entry Decelerator Systems and Flight Mechanics.

* Development Engineer, Analytics Department.

† Associate Professor, Department of Aeronautical and Astronautical Engineering. Associate Fellow AIAA.

‡ TM, Goodyear Aerospace Corporation, Akron, Ohio.

Introduction

A LONG-TERM development program has been in progress that has as a basic objective the development of the capability for predicting the aerodynamic drag and static stability coefficients of a decelerator residing in the wake of a forebody. Under this program, attention has been given to the development of methods for predicting the properties of the forebody viscous and inviscid wake flowfield, which serves as the effective freestream for the decelerator.[1]

Recently, efforts have been completed under which methods were developed to define the flowfields into and around supersonic decelerators of both the porous (e.g., a parachute) and the nonporous (e.g., Ballute) types and at zero angle of attack. With solutions for the decelerator flowfield, it is then possible to perform drag computations, using the pressure distributions as obtained from the flowfield calculations.

Summary of Viscous and Inviscid Wake Flow Methods

In order to determine the decelerator flowfield in a supersonic flow, it is necessary first to know the nonuniform viscous and inviscid wake flowfield, which serves as an effective freestream for the decelerator (see Fig. 1). The fundamental assumption utilized in developing the viscous wake characteristics for a given forebody is that the wake momentum defect at any axial distance downstream of the forebody is equal to the integrated boundary-layer momentum defect at the base of the forebody.[1,2] This assumption provides a direct link between the viscous wake properties and the forebody configuration; thus, any attempt to predict the viscous wake behind a body must begin with some knowledge of the forebody boundary layer, including whether this flow is laminar or turbulent.

After the forebody boundary-layer characteristics have been determined, the boundary-layer momentum defect is then equated to the momentum defect of the viscous wake. At this point, one must determine whether the wake is laminar or turbulent. Obviously, if the forebody boundary layer is turbulent, then the wake also will be turbulent. However, if the forebody boundary layer is laminar, then the viscous wake may be either laminar or turbulent, depending on whether wake transition occurs. If the wake is laminar, a "cylindrical" wake model is used to approximate the actual wake.

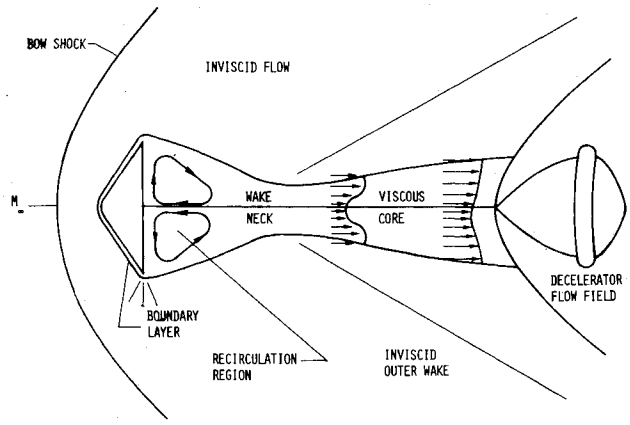

Fig. 1 Basic flow structure.

If the wake is turbulent, the no-slip boundary condition is satisfied across a thin sublayer and the outer viscous wake profiles can be calculated using the mathematical formulation for a conventional turbulent wake.

Once the wake is determined to be either laminar or turbulent, the viscous wake solution can be carried out. The starting point for the viscous wake solution is considered to be at the wake neck location or at the rear stagnation point. Calculations then can be made for any axial position downstream of the starting point.

For the inviscid wake solution in a supersonic flow, a mass flow balance calculation procedure is used. It is required that the shape of the forebody shock wave and the freestream conditions be known to carry out this calculation.

Once the viscous and inviscid wake radial profiles are known as a function of the distance downstream of the forebody base, the effective freestream environment for the decelerator has been defined. The next step is to compute the flowfield and pressure distribution over the decelerator. This surface pressure distribution then can be used as part of a decelerator drag calculation.

Decelerator Flowfield

Internal Flowfield Solution

Figure 2 presents the flowfield around a supersonic parachute. As shown, the flowfield logically divides itself into an external and an internal part. The external flow consists of that part of the flow which passes around the outside of the parachute; the internal flow is that portion of the flow which passes through the parachute.

The internal flow will be subsonic since it is the result of flow across the nearly normal portion of the decelerator bow-shock wave. To analyze the internal flow, it is necessary to bound this flow region by what will be called the dividing streamline. To calculate the dividing streamline, a mass flow balance is used that relates the mass flow through the parachute roof to the same mass flow passing through the bow shock. Using the stream function ψ_D to identify the dividing streamline gives

$$\psi_D = 2\pi \int_0^{R_s} (\rho V)_w r dr = \int_0^{S_p} (\rho V)_r \lambda dS \qquad (1)$$

where R_s is the radial location on the bow shock wave through which the dividing streamline passes and $(\rho V)_w$ is the local mass flow rate at a radial position (r) immediately upstream of the shock front (for a trailing decelerator, this is specified by the wake flow). This relation is also used to find the position of an interior streamline on passage through the shock to the position of the same streamline at the parachute roof having area S.

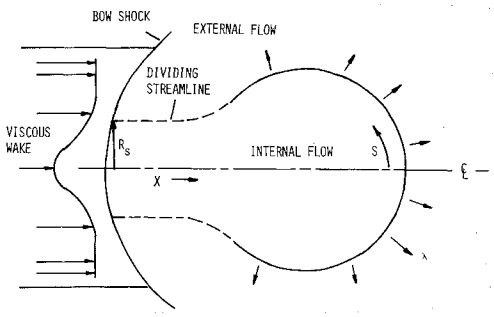

Fig. 2 Supersonic flowfield for a porous parachute.

Using Eq. (1) along with a suitable number of streamlines, the canopy internal pressure distribution can be found by assuming that the local internal canopy pressure is due to the stagnation of the flow along a streamline and thus will be equal to the local total pressure on that streamline.

External Flowfield Solution

The method to be outlined here is directly applicable to the problem of calculating the flowfield around a supersonic decelerator of the Ballute type. In addition, this method also can be used to calculate the external flow around a parachute. In formulating a method for external flowfield calculations, it was found convenient to follow Maslen[3] and consider an inverse method of calculation in which the resulting flowfield and body shape are generated from the governing equations.

Maslen derived a set of equations for an inviscid gas flow in a curvilinear coordinate system using a Von Mises transformation. The equations were simplified for the hypersonic flow case in which the layer of gas between the shock and the body is thin and the flow is approximately parallel to the surface except near the stagnation point. Under these assumptions, Maslen obtained a series of transformed equations in which flow properties along streamlines could be calculated. He showed that the variation of pressure distribution between streamlines could be obtained directly from the momentum equation using the properties at the shock wave and the shock wave radius of curvature. Upon integrating the momentum equation, he obtained the pressure distribution across the shock layer.

Similarly, other flow properties were evaluated under the assumption of isentropic flow along individual streamlines. Once the flow properties had been calculated, Maslen transformed back to a physical coordinate system. His solution was thus complete within the hypersonic flow assumptions specified.

However, the present interest in this method lies in the low and intermediate supersonic region and, for such conditions (i.e., low Mach numbers), the assumption of parallel flow no longer applies. One must then return to the full form of the momentum equation normal to a streamline. Following a suggestion made by Maslen, an iterative procedure was developed in which the first approximation corresponded to that outlined previously. One then proceeds to improve on this with subsequent iterations. These start with a calculation of normal velocity through a Von Mises transformation knowing the total velocity from the first approximation. A new calculation of the pressure gradient can now be made from the full form of the momentum equation. This equation can then be numerically integrated to get the pressure; a new calculation of the velocities then follows directly from the energy equation. With this, a new pressure gradient can be calculated, and the entire procedure is repeated until a suitable degree of convergence is obtained.

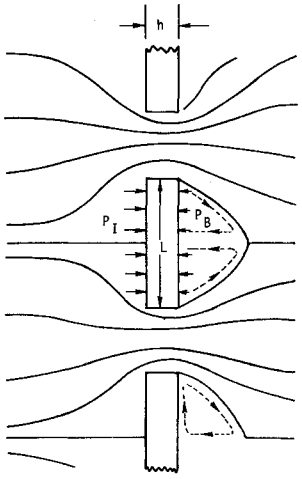

Fig. 3 Model flow through parachute material

An important consideration that has not yet been really discussed for each flowfield calculation method presented here is the inclusion of variable freestream, or upstream, properties. This aspect of flowfield calculations is particularly important in carrying out calculations of the flowfields for trailing decelerators. Decelerators trailing a forebody are normally immersed in a wake that is characterized by nonuniform variations in velocity, density, and other properties in a direction normal to the wake centerline. Because of the variable upstream properties, the proper upstream velocity, Mach number, and total temperature must be calculated separately at each shock wave point. Furthermore, both total temperature and total pressure, while constant along a streamline downstream of the shock wave, will differ from streamline to streamline.

Once the wake properties have been defined, a flowfield calculation can be made. In carrying out this calculation, a suitable number of streamline increments must be selected that will adequately define the body shape desired.

The important result of this flowfield calculation is the pressure distribution required for a drag calculation. In addition to pressure distribution, this method will also predict approximate temperature distributions, local Mach numbers, and local velocities on each streamline considered.

Drag Prediction Methods

Drag Prediction for Parachute-Type Decelerators

The first step in the drag calculation procedure is to define the shape of the bow shock wave generated by the decelerator. After this is known, one can then calculate the location of the dividing streamline on the bow shock wave and proceed with the inner flowfield calculations. The inner flow is divided into a number of streamlines at the bow shock; thus, one needs only to determine where each streamline passes through the parachute roof and what the resultant pressure distribution is with respect to the flow of each streamline. If it is assumed that the porosity of a parachute can be represented by a network of rectangular material elements of negligible thickness ($h/L \ll 1$ as shown in Fig. 3), then one need only consider the pressure on the forward facing side P_I, and on the base P_B. The drag of the parachute can then be expressed as:

$$\text{Drag} = \int_0^{S_p} (P_I - P_B)(1 - \lambda) \sin\left(\tan^{-1}\frac{dr_B}{dx}\right) dS \quad (2)$$

Here, dS is an increment in roof area measured from the axis of symmetry. The effective porosity λ must be specified as a function of S. In doing this, the location of vents, slots, and etc. can be taken into account. In addition, dr_B/dx must be specified as a function of S and the pressure difference $(P_I - P_B)$ as a function of the stream function value ψ, which in turn is calculated as a function of S. The unknown thus is the relationship between the pressure difference $(P_I - P_B)$ and ψ.

Now P_I can be readily evaluated by assuming the streamline stagnates on each material element and thus $P_I = P_t(\psi)$, where $P_t(\psi)$ is the local total pressure for each streamline associated with the nonuniform wake flow properties ahead of the decelerator bow shock. After the interior canopy pressure distribution is defined, the next step is to calculate the base pressure P_B. Assuming choked flow at the parachute roof and defining a base pressure coefficient as

$$C_{P_*} = (P_B/P_* - 1)/(\gamma/2)M_*^2 \quad (3)$$

where the reference conditions P_* and M_* are the choked flow conditions at the parachute roof, then this equation can be rewritten in the form

$$C_{P_*} = \frac{[(\gamma + 1)/2]^{\gamma/\gamma-1}(P_B/P_t) - 1}{\gamma/2} \quad (4)$$

An appropriate estimate of $C_{P_{B\infty}}$ can be obtained by examining the limited amount of data available from the University of Minnesota[4] as shown in Fig. 4 where $C_{P_{B\infty}}$ is presented as a function of M_∞, the effective freestream Mach number, i.e., the Mach number just upstream of the parachute bow shock. For the case of a forebody, this Mach number was based on viscous wake flow calculations. $C_{P_{B\infty}}$ is defined and related to Eqs. (3) and (4) by

$$C_{P_{B\infty}} = (P_B/P_\infty - 1)/(\gamma/2)M_\infty^2 =$$
$$\left\{\frac{P_{t_2}}{P_\infty}\left[\left(\frac{\gamma+1}{2}\right)^{-\gamma/\gamma-1}\left(1 + \frac{\gamma}{2}C_{P_*}\right)\right] - 1\right\}\frac{2}{\gamma M_\infty^2} \quad (5)$$

where P_{t_2} is the total pressure downstream of the parachute bow shock wave and all data are for flow through the normal or near-normal portions of the shock wave. As seen in Fig. 4, there is in general a fair correlation with the University of Minnesota[4] data for an assumed $C_{P_*} = -1.0$. Using this value of C_{P_*} and expressing the nondimensional pressure difference as

$$\Delta P/P_t = (P_I - P_B)/P_t$$
$$= 1 - [(\gamma + 1)/2]^{-\gamma/\gamma-1}[1 + (\gamma/2)C_{P_*}] \quad (6)$$

the drag then can be calculated directly from Eq. (2).

Drag Prediction for Ballute Decelerators

For a Ballute, the drag is divided into the three following components: 1) forebody pressure drag, 2) burble fence drag, and 3) base-pressure drag. The forebody pressure drag is obtained by integrating the pressure distribution as computed by the external flowfield technique discussed earlier.

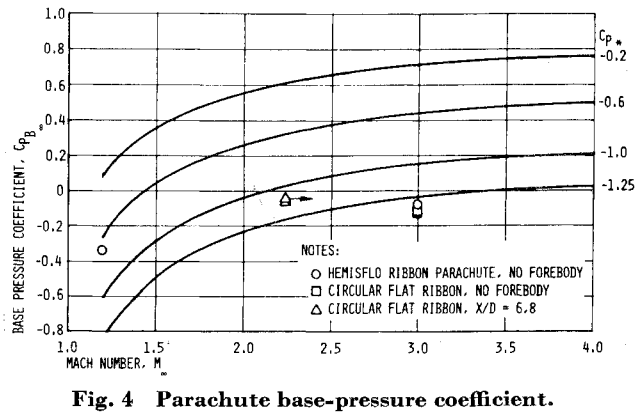

Fig. 4 Parachute base-pressure coefficient.

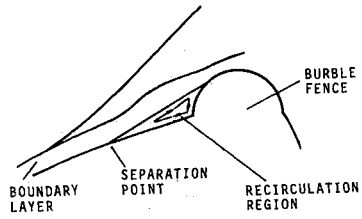

Fig. 5 Boundary-layer separation ahead of burble fence.

In calculating the forebody pressure drag, it should be recognized that there is a pressure rise associated with the boundary layer. As may be seen from the flowfield in Fig. 5, the boundary layer is forced to separate, and the resulting flow pattern is much like that over a forward facing step. Gadd[5] has examined this type of problem in terms of the prediction of plateau pressure levels associated with turbulent boundary-layer separation. He found that the pressure rise at separation is just sufficient to stagnate this streamline to form the recirculation region shown in Fig. 5. For a trailing Ballute, it can be shown that the boundary layer is usually turbulent since the wake a Ballute resides in is generally turbulent. However, Ballutes tested without a forebody sometimes show a laminar separation. In either case, this pressure rise is of only minor importance in terms of the forebody pressure drag.

It is important, however, as part of the second contribution to the drag of a Ballute, i.e., the burble fence drag. Here, it is the plateau pressure that is of interest since this is the pressure over most of the burble fence. It is also in general the peak pressure since, after reattachment, the flow expands around the burble fence with a subsequent pressure drop.

Figure 6 is a comparison of experimental data and the theoretical pressure rise coefficient for turbulent boundary-layer separation near a burble fence on a Ballute. Gadd's equation

$$\frac{P_s}{P_1} = \left(\frac{1 + [(\gamma - 1)/2]M_1^2}{1 + 0.64[(\gamma - 1)/2]M_1^2}\right)^{\gamma/\gamma-1} \tag{7}$$

where P_s is the plateau pressure, P_1 is the local pressure at separation, and M_1 is the local Mach number at separation, is shown. Fair agreement with experimental data is evident. Figure 6 also shows a laminar separation prediction of Gadd given by

$$C_{P_s} = 1.90(M_1^2 - 1)^{-1/4}Re_1^{-1/4} \tag{8}$$

which has been compared with data for Ballutes having no forebody.

It should be noted that a laminar boundary-layer separation, if it occurs, is most likely to occur for a Ballute residing in a laminar wake or for a Ballute having no forebody. For the turbulent boundary-layer separation case, the pressure rise level is independent of Reynolds number. This independence was noted by Gadd, and data validating this conclusion is shown in Ref. 5.

Thus the drag on the front of the burble fence drag can be computed using either Eqs. (8) or (9), depending on whether the boundary-layer separation is laminar or turbulent. The drag on the back side of the burble fence is treated next as part of the third and final contribution to the drag.

The third contribution to Ballute drag is the base-pressure drag. Here, a correlation of experimental data must be considered. As seen in Fig. 7, the correlation

$$C_{P_B} = -1.0/M(_\infty^2 + 0.7) \tag{9}$$

correlates quite well with experimental data. This correlation appears to be independent of the presence of a forebody. The base pressure appears to be primarily fixed by the interaction of the inviscid wake with the decelerator. Since the inviscid wake is at a near freestream condition, it is M_∞ that correlates the data.

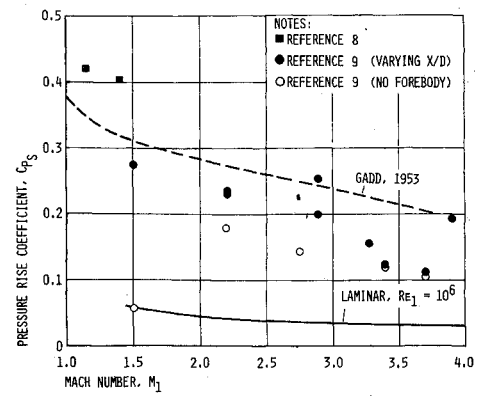

Fig. 6 Comparison of experimental data and theoretical pressure-rise coefficient.

Drag Results for Parachute-Type Decelerators

Drag computations have been made for several geometrically porous parachute configurations using the internal flowfield analysis discussed earlier. The results of drag computations for three parachute configurations will be presented. These include 1) a circular flat-ribbon parachute ($\lambda_g = 25\%$) with no forebody and no suspension lines; 2) a circular flat-ribbon parachute ($\lambda_g = 20\%$) with no suspension lines at an X/D of 6 calibers aft of an ogive forebody; 3) a reefed hemisflo parachute ($\lambda_g = 17\%$ with no forebody and no suspension lines ($d_R/d_0 = 0.3$). These configurations were selected for analysis because of the availability of well-defined bow shock shapes.

Figure 8 presents a typical flowfield about the circular flat-ribbon parachute at an X/D of 6.0 behind an ogive forebody in a Mach 3.0 freestream and shows the network of streamlines for the external flowfield. The bottom streamline corresponds to the dividing streamline, which separates the internal and external flow. In calculating a parachute frontal drag coefficient, the internal flowfield solution has been used entirely since it is the interior canopy pressure distribution that produces the major component of the parachute drag.

In calculating an interior parachute pressure distribution, the flowfield was divided into 20 radial streamline increments at the bow shock wave. The properties of each streamline ahead of the shock depend on the freestream environment or the effective nonuniform freestream if the bow shock resides in the wake of a forebody. The resulting distribution of the streamlines on the parachute roof depend on the given para-

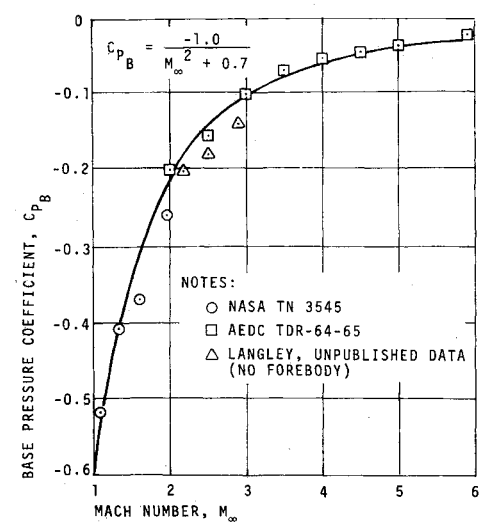

Fig. 7 Ballute base-pressure coefficient.

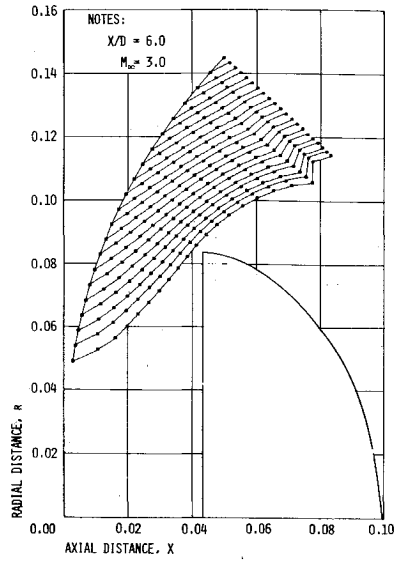

Fig. 8 External flowfield for circular flat-ribbon parachute.

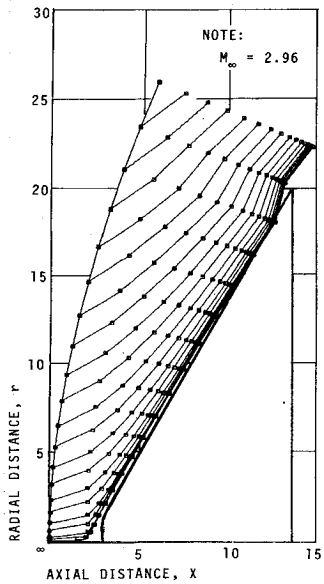

Fig. 10 Flowfield for blunted 120° cone.

chute's porosity λ; that is, the mass flow through the parachute may vary at different radial stations depending on the local porosity.

Figure 9 presents some typical interior canopy pressure distributions as calculated by the present method. Also presented are the experimental pressure distributions of Ref. 4. Excellent agreement between experimental and theoretical calculations is shown for the circular flat-ribbon parachute in which no forebody is present. Some disagreement does exist for this parachute when the effect of the variable wake properties is introduced. However, these differences do not significantly alter the resulting drag coefficient. Integration of the interior pressure distribution in conjunction with empirical relations for the base-pressure distribution has resulted in the predicted parachute drag coefficients given in Table 1.

Of particular significance is the effect of the forebody wake on the drag coefficient for the circular flat-ribbon parachute. The drag of a given parachute can be significantly reduced if the wake is of a significant size in relation to the canopy size. This is because the internal canopy flow in some instances is comprised primarily of a wake flow that generally has a lower total pressure behind the bow shock than if no wake was present.

Ballute Drag Results

A check on the external flowfield calculation procedure was first made by comparing its results with those obtained from Taylor-Maccoll theory for a pointed cone in a supersonic flow. The results obtained using the flowfield calculation procedure were in excellent agreement with the predictions of Taylor-Maccoll. A further check on the external flowfield method was then made by calculating the flowfield for a 120° blunted cone at Mach numbers of 2.96 and 4.63. The resulting flowfield for one of these cases is shown as a network of streamlines in Fig. 10 where the zero streamline corresponds to the 120° cone shape. The resultant pressure distribution on the zero streamline in both cases compared favorably with experimental data.[6,7] These favorable comparisons have suggested the use of this method in calculating the drag coefficient for a trailing Ballute decelerator.

A Ballute behind an ogive forebody at $M_\infty = 1.76$ was selected as the initial decelerator for drag computations. This Ballute had a reasonably well-defined shock shape (unpublished data) at X/D stations behind the forebody of 7.6 and 10.0. Prior to performing flowfield calculations, viscous and inviscid wake profiles were generated using the techniques described in Refs. 1 and 2.

With these effective freestream conditions and the Ballute shock shapes known, a calculation of the external flowfield was made for each of the noted X/D's with the aim being to

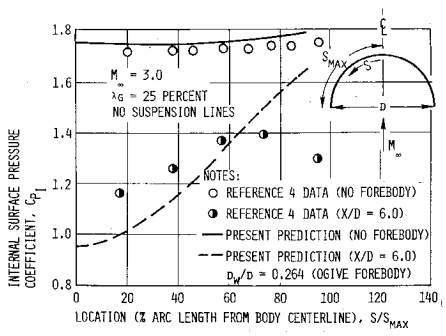

Fig. 9 Internal pressure coefficient on circular flat-ribbon parachute.

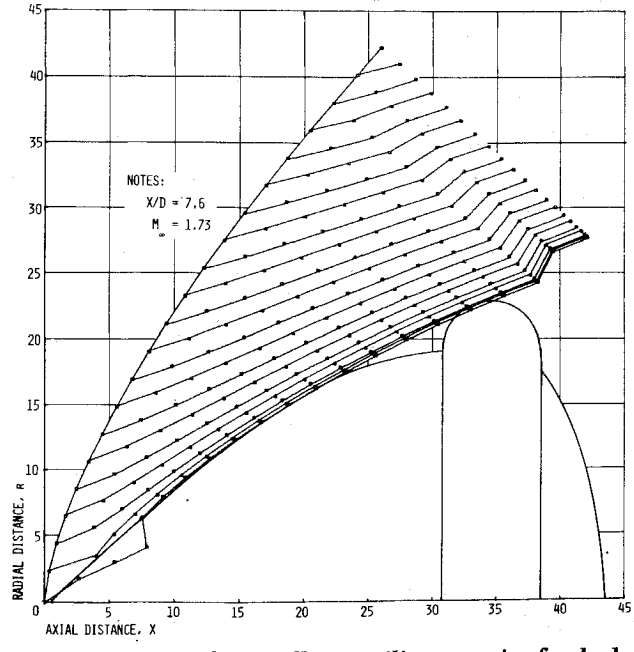

Fig. 11 Flowfield for a Ballute trailing an ogive forebody.

Table 1 Drag results on parachutes

Parachute	Present method			Ref. 4 data		
	C_{DI}	C_{DE}	C_{D_0P}	C_{DI}	C_{DE}	C_{D_0P}
Circular flat-ribbon (no forebody)	0.819	0.011	0.830	0.802	0.042	0.844
Circular flat-ribbon (X/D = 6.0, d_w/d_P = 0.264)	0.585	0.011	0.596	0.564	0.033	0.597
Reefed hemisflo (d_R/d_0 = 0.3, no forebody)	0.107	0.044	0.151	0.116	0.036	0.152

predict a body streamline shape which is coincident with that of a Ballute.

These calculations showed that slight variations in shock shape could affect the resulting body shape calculations and that an iteration on shock shape would be necessary to define the Ballute shape satisfactorily. Such iterations on a known shock shape, when required, have been found to be normally within the accuracy of reading the coordinates of the originally given shock shape. Of course, if no shock shape is available, a number of iterations may be required to obtain the desired body shape. An iteration of the shock shape was conducted on both of the aforementioned Ballute cases until the criteria established for the Ballute were satisfied. These criteria were as follows: 1) the body streamline should separate near the Ballute maximum diameter and reattach near the center of the Ballute burble fence; 2) since an inverse method of solution is being used, the resulting body shape must be a close resemblance of a Ballute.

Figure 11 is an example of a typical flowfield solution satisfying the above criteria. In this instance, the coarse mesh size fo the numerical calculation procedure limits the accuracy of the results in the nose region; however, over the rest of the body, the results appear reasonable. Once the flowfield is determined, the pressure distribution for the body streamline is integrated to define a drag coefficient over the forward face of the Ballute. A typical body streamline pressure distribution for a Ballute is compared in Fig. 12 with experimental data at Mach numbers similar to those under present consideration.[8,9] Reasonable agreement can be seen to exist over most of the forebody except in the nose region where, because of the tow cable in the wind-tunnel test, there is a separated flow and the experimental pressures are lower than predicted.

Calculations of the total Ballute drag coefficient were made. The results in Table 2 were obtained for the Ballute at an X/D of 7.6.

These results are plotted in Fig. 13 and show that the present drag prediction method using the modified Maslen method along with the burble fence and base drag correlations does indeed give results consistent with experiment. Note, however, that the base drag coefficient for all Ballutes has been calculated using the correlation given in Eq. (10). The method of Gadd for a forward facing step does appear to give an estimate of the burble fence drag and the plateau pressure just ahead of the burble fence. Based on these results, additional Ballute drag calculations were made to investigate the effect of decelerator/forebody diameter ratio, and Mach number. These results are shown in Table 3.

The results in Table 3 from Ballutes 1 and 2 show a reduction in drag coefficient with decreasing decelerator/forebody diameter ratios. The drag loss seen here is related to the reduction in average dynamic pressure, which the Ballute sees as the wake size is increased relative to the decelerator size. The effect of decelerator X/D location is shown from the drag results obtained on Ballutes 1 and 3. This comparison points out that the decelerator drag coefficient will increase as it sees higher average dynamic pressures, which occur for increasing axial distance downstream of the forebody.

The effect of Mach number is illustrated by the results obtained on Ballutes 1 and 4. It is seen that the predominant loss in drag at higher Mach numbers is attributed to the decrease in base pressure drag. Also shown is an integration of the Ballute 5 pressure distribution as obtained at Arnold Engineering Development Center, which shows fairly good agreement with the results obtained from the present method.

Table 2 Ballute drag results (X/D = 7.6)

Balute	M	C_{DF}	C_{DBF}	C_{BD}	C_{D_0T}
Present method	1.73	0.650	0.380	0.270	1.300
Lewis data[8]	1.57	0.639	0.438	0.316	1.438
Lewis data[8]	1.96	0.638	0.377	0.220	1.238
AEDC data[9]	2.00	0.556	0.375	0.213	1.144

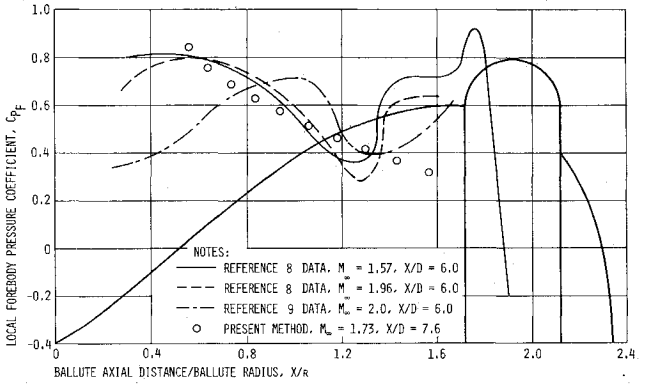

Fig. 12 Comparison of theoretical and experimental pressure distribution over forward face of trailing Ballute.

These Ballute drag coefficients have been compared with some experimental and flight test results. This comparison is shown in Fig. 14, and the agreement is considered good. It is recognized that the number of configurations and flow conditions studied is limited; however, these results demonstrate the application of the present drag prediction method to Ballute decelerators.

Summary

A method of calculation has been developed to predict the flowfield and resultant drag coefficient for nonporous trailing

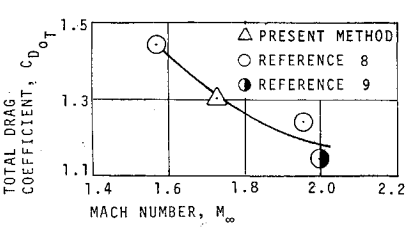

Fig. 13 Comparison of initial Ballute drag-coefficient calculation with experimental data.

Table 3 Calculated drag on ballutes having 10% burble fences using present method[a]

Ballute	d/D	M	X/D	C_{DF}	C_{DBF}	C_{DB}	C_{D_0T}
1	3.8	1.73	7.6	0.65	0.38	0.27	1.30
2	1.0	1.73	7.6	0.61	0.39	0.27	1.27
3	3.8	1.73	10.0	0.67	0.40	0.27	1.34
4	3.8	3.00	5.2	0.64	0.33	0.10	1.07
5[b]	3.8	3.00	5.2	0.56	0.27	0.10	0.93

[a] Reference area = $r_{F_{max}}{}^2$.
[b] AEDC wind-tunnel data.[9]

decelerators such as a Ballute using forebody wake profiles as effective freestream conditions. Results obtained using this drag predictive method have been compared with experimental data, and good agreement has been shown to exist over a range of freestream Mach numbers and decelerator axial locations aft of the forebody base. Results using a parachute drag predictive method have also been encouraging. These methods offer one the ability to predict a given decelerator's drag characteristics rapidly in the supersonic flow regime knowing only the forebody-decelerator geometry and to investigate decelerator performance parametrically.

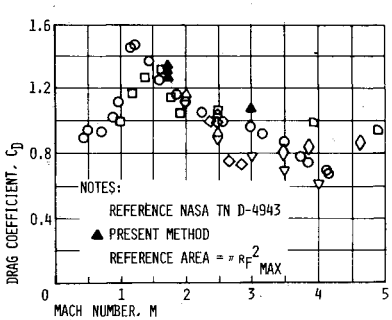

Fig. 14 Ballute drag coefficient.

References

[1] Nerem, R. M. and Henke, D. W., "Theoretical and Experimental Studies of Supersonic Turbulent Wakes and Parachute Performance," AIAA Paper 68-947, El Centro, Calif., 1968.

[2] Henke, D. W., "Establishment of an Unsymmetrical Wake Test Capability for Aerodynamic Decelerators, Vol. II: Analysis of High Speed Axisymmetric Wakes and Parasonic Parachute Performance," AFFDL-TR-67-192, March 1968, Air Force Flight Dynamics Lab., Dayton, Ohio.

[3] Maslen, S. H., "Inviscid Hypersonic Flow Past Smooth Symmetric Bodies," *AIAA Journal*, Vol. 2, No. 6, June 1964, pp. 1055–1061.

[4] Niccum, R. J., Goar, K. J., and Lenius, W. W., "Experimental Determination of Transonic and Supersonic Pressure Distribution and Mass Flow Accommodation for Ribbon Parachutes During Inflation," Vol. II, AFFDL-TR-65-105, Dec. 1965, Air Force Flight Dynamics Lab., Dayton, Ohio.

[5] Gadd, G. E., "Interactions Between Wholly Laminar or Wholly Turbulent Boundary Layers and Shock Waves Strong Enough to Cause Separation," *Journal of Aeronautical Sciences*, Vol. 20, No. 11, Nov. 1965, pp. 729–739.

[6] South, J. C., Jr., "Calculation of Axisymmetric Supersonic Flow Past Blunt Bodies with Sonic Corners, Including a Program Description and Listing," TN D-4563, May 1968, NASA.

[7] Stallings, R. L., Jr. and Tudor, D. H., "Experimental Pressure Distributions on a 120-Deg Cone at Mach Numbers from 2.96 to 4.63 and Angles of Attack from 0 to 20 Deg," TN-D-5054, March 1969, NASA.

[8] Turk, R. A., "Pressure Measurements on Rigid Model of Ballute Decelerator at Mach Numbers from 0.56 to 1.96," TN D-3545, March 1966, NASA.

[9] Bell, R. R., "Pressure Measurements on the Rigid Model of a Balloon Decelerator in the Wake of a Simulated Missile Payload at Mach Numbers 1.5 to 6.0," AEDC TD R-6465, April 1964, Arnold Engineering Development Center, Tenn.